Contents lists available at ScienceDirect

Colloids and Surfaces B: Biointerfaces

journal homepage: www.elsevier.com/locate/colsurfb

Biosynthesis and physico-chemical characterization of high performing peptide hydrogels@graphene oxide composites

Laura Chronopoulou [a], Antonio Di Nitto [a], Massimiliano Papi [b], Ornella Parolini [b], Mirella Falconi [c], Gabriella Teti [c], Aurelio Muttini [d], Wanda Lattanzi [b], Valentina Palmieri [b], Gabriele Ciasca [b], Alessandra Del Giudice [a], Luciano Galantini [a], Robertino Zanoni [a], Cleofe Palocci [a,e,*]

[a] *Department of Chemistry, University of Rome La Sapienza, Italy*
[b] *Fondazione Policlinico Universitario A. Gemelli IRCSS, Rome, Italy*
[c] *Department of Biomedical and Neuromotor Sciences, University of Bologna, Italy*
[d] *Faculty of Bioscience and Agro-Food and Environmental Technology, University of Teramo, Italy*
[e] *CIABC, University of Rome La Sapienza, Italy*

ARTICLE INFO

ABSTRACT

Hydrogels based on short peptide molecules are interesting biomaterials with wide present and prospective use in biotechnologies. A well-known possible drawback of these materials can be their limited mechanical performance. In order to overcome this problem, we prepared Fmoc-Phe$_3$ self-assembling peptides by a biocatalytic approach, and we reinforced the hydrogel with graphene oxide nanosheets. The formulation here proposed confers to the hydrogel additional physicochemical properties without hampering peptide self-assembly. We investigated in depth the effect of nanocarbon morphology on hydrogel properties (i.e. morphology, viscoelastic properties, stiffness, resistance to an applied stress). In view of further developments towards possible clinical applications, we have preliminarily tested the biocompatibility of the composites. Our results showed that the innovative hydrogel composite formulation based on FmocPhe3 and GO is a biomaterial with improved mechanical properties that appears suitable for the development of biotechnological applications.

1. Introduction

In the last decades, in order to develop delivery strategies for targeted therapies, research has focused not only on the discovery of new bioactive molecules, but also on how drugs can be administered [1–3]. A promising strategy is the implantation of drug delivery depots in the target site, allowing bioactive molecules entrapped in the device to be released over time [4]. In the past this kind of implantation was surgical but now, thanks to the design of new materials, the injection through a needle in the injured site is emerging [1]. In general, the material must be biocompatible, biodegradable, like its degradation products, have good mechanical properties and appropriate porosity [5,6].

Self-assembling hydrogels are exploitable materials that can be injected in their liquid phase [1,6–11]. Also short peptides can act as hydrogelators, self-assembling into supramolecular structures [12–16]. It is common to use peptides for biomedical purposes because they are

biocompatible, cheap, easily prepared and functionalized [12]. One limitation is the poor mechanical performance, which prompts the search for alternative procedures, such as the use of nanofillers [17]. Graphene oxide (GO), the oxidized form of Graphene, has versatile applications given by its optimal mechanical and isolating properties, its inexpensiveness and dispersability in water [18]. GO has a planar structure with epoxy, carbonyl, carboxylic and hydroxyl groups on both sides of the basal plane and on the borders [19,20], enabling GO to interact with many molecules through hydrophobic or hydrophilic interactions [21]. Recent works have demonstrated the possibility to introduce GO as nanofiller in peptide based gels [17,22,23]. GO did not hinder gel formation in the studied systems, and it was useful for improving mechanical properties. In our work we evaluated the possibility to obtain a novel injectable composite peptide hydrogel using GO as nanofiller [24,25]. *Pseudomonas fluorescens* lipase was used to catalyze the synthesis of FmocPhe3 that acts as a hydrogelator. In a first

---

phase of the work, we engaged in studying how the presence of GO nanofillers in the native structure of the hydrogel may influence FmocPhe3 synthesis, its ability to self-assemble into nanofibers and its viscoelastic properties. This work was aimed at developing composite materials with tailored mechanical properties for future *in vivo* biomedical applications. In view of further developments towards a possible translation to clinical applications, we have measured the production of reactive oxygen species by blood monocytes, as a preliminary assessment of the toxicity of the composites.

2. Materials and methods

2.1. Materials

Fluorenylmethyloxycarbonyl-phenylalanine (FmocPhe, >99 %) and diphenylalanine (Phe2, >99 %) were purchased from Bachem GmbH (Weil am Rhein, Germany) and used as received. Graphene oxide water dispersion (GO, 0.4 wt % concentration) was purchased from Graphenea Inc. (Cambridge, MA, USA). Lipase from *Pseudomonas fluorescens* (PFL, ≥20.000 U/mg) and all other chemicals and solvents were obtained from Sigma Aldrich (St. Louis, MO, USA) and used as received.

2.2. Biosynthesis of fmoc-tripeptide hydrogels

FmocPhe and Phe2 were added in equimolar quantities to a mixture containing 1 mL of water or 1 mL of GO in water and 420 μL of 0.5 M NaOH, and stirred magnetically for 10 min. Three different GO concentrations were used: 0.01 mg/mL, 0.1 mg/mL and 1 mg/mL. Then, pH was adjusted to 7 by the addition of 1.5 mL of 0.1 M HCl. PFL solution (50 mg/mL) was added (100 μL) and the reaction mixture was incubated at 30 °C for 30 min.

2.3. Rheological measurements

The kinetics of hydrogel formation were studied with an Anton Paar MCR 302 rotational rheometer, following the elastic (G') and viscous (G'') modules trend over time. The instrument, equipped with a temperature control unit, was used with aplate-plate geometry. The gelation process was followed at 30 °C, applying a deformation of 1% and a constant frequency of 1 Hz. The elastic and viscous modules of preformed hydrogels were measured in frequency sweep experiments, varying the applied frequency in the range of 0.01–20 Hz, at constant temperature (30 °C). For recovery tests, the measurements were conducted on preformed hydrogels applying a shear stress of 1 Pa and a frequency of 1 Hz for 5 min, before applying increasing stress values (50, 100, 150, 200 Pa) for 30 s with 5 min intervals for recovery.

2.4. Saxs analysis

The X-ray scattering measurements were performed at SAXSLab Sapienza with a Xeuss 2.0 Q Xoom system (Xenocs SA, Sassenage, France) equipped with a micro-focus Genix 3D X-ray Cu source ($\lambda = 0.1542$ nm), a two-dimensional Pilatus3 R 300 K detector placed at variable distance from the sample and an additional Pilatus3 R 100 K detector at fixed shorter distance (Dectris Ltd., Baden, Switzerland). Measurements were performed at room temperature ($25 +-1$ °C) and in vacuo (<0.2 mbar), with three different sample-detector distances, in order to record the sample scattering within the scattering vector range of $0.045 < q < 32$ nm^{-1}($q = 4\pi\sin(\theta)/\lambda$, where 2θ is the scattering angle). Samples were loaded within 1 min after PFL addition into vacuum-tight cells having 50 μm-thick Kapton windows and 1-mm spacers. A cell loaded with water and an empty cell were used for background subtraction. The two-dimensional scattering patterns were subtracted for the "dark" counts, and then masked, azimuthally averaged and normalized for transmitted beam intensity, exposure time and subtended solid angle per pixel, by using the FoxTrot software

developed at SOLEIL. The one-dimensional intensity vs. q profiles were subtracted for the contributions of the solvent and cell windows, using the peak of liquid water at 20 nm^{-1} in the WAXS to scale the water content to be subtracted. Model calculations of scattering profiles were performed using the software SasView [www.sasview.org]. Pair distance distributions of the cross-section of elongated objects were obtained by indirect Fourier inversion of the I(q)·q profiles performed with the software BayesApp [26].

2.5. XPS analysis

X-ray photoelectron spectroscopy (XPS) measurements were obtained from a modified Omicron NanoTechnology MXPS system. Spectra were excited by achromatic Mg Kα and Al Kα photons (hν = 1253.6 and 1486.6 eV, respectively), generated operating the anode at 14–15 kV, 10–20 mA. The samples were mounted on freshly cleaved graphite. Experimental spectra were theoretically reconstructed by fitting the peaks to symmetric pseudo-Voigt functions (linear combination of gaussian and lorentzian peaks) and the background to a Shirley or a linear function. XPS atomic ratios between relevant core lines were estimated from experimentally determined area ratios, corrected for the corresponding theoretical cross sections and for a square root dependence of the photoelectrons kinetic energies. All binding energies were referenced to the most intense C1s peak (285.0 eV). Samples were measured on stainless steel tips covered with either freshly cleaved graphite foil or Teflon. In the first case, a small correction for static charging under X-rays was applied, and more defined C1s, N1s and O1s spectra were obtained, which were used for curve fitting analysis. In the second case, any contribution from the tip was removed from the portion of the spectrum due to the C1s, N1s and O1s peaks of the sample.

2.6. NMR Spectrometry

Hydrogel composites were suspended in a mixture of H2O and D2O (9:1 v/v) and analyzed by ^{1}H NMR at 298 K on a Bruker AVANCE III spectrometer at 9.4 T operating at the frequency of 400.13 MHz, equipped with a Bruker multinuclear z-gradient inverse probe head. Spectra were acquired employing the standard preset pulse sequence for solvent suppression (scan number 64 transients, recycle delay 9.5 s, spectral width 15 ppm, 64 K data points, total acquisition time 15 s).

2.7. AFM measurements

Samples underwent indentation-type AFM analysis immediately after preparation. All measurements were performed in deionized water at room temperature using a Nanowizard II atomic force microscope (JPK Instruments AG, Berlin, Germany) mounted on an optical microscope (Axio Observer Carl Zeiss, Oberkochen, Germany). MikroMashCSC-37 silicon cantilevers (tip radius: 10 nm, nominal spring constant: 0.3 N/m) were used. The cantilever spring constant was determined by thermal calibration before each measurement. Mechanical properties were measured through the acquisition of Force-Distance (FD) curves using an indentation force of 4 nN at 2 μm/s indentation speed. The Young's modulus E of the sample was retrieved fitting each force distance curve with the JPK software, using the Sneddon model for conical indenters: $F(\delta) = \frac{2E \tan(\alpha)}{\pi(1-\nu 2)} \delta^2$ (α: half-aperture angle of the conic tip, δ: indentation depth, ν: Poisson ratio). FD curves were measured in different sample locations, three replicates were performed and the results were averaged.

2.8. TEM and SEM measurements

A drop of each sample was deposited on a grid (300 mesh Cu-grid), carbon-coated and stained with a 2% uranyl acetate solution for 30 s in the dark at room temperature, allowed to dry under vacuum and
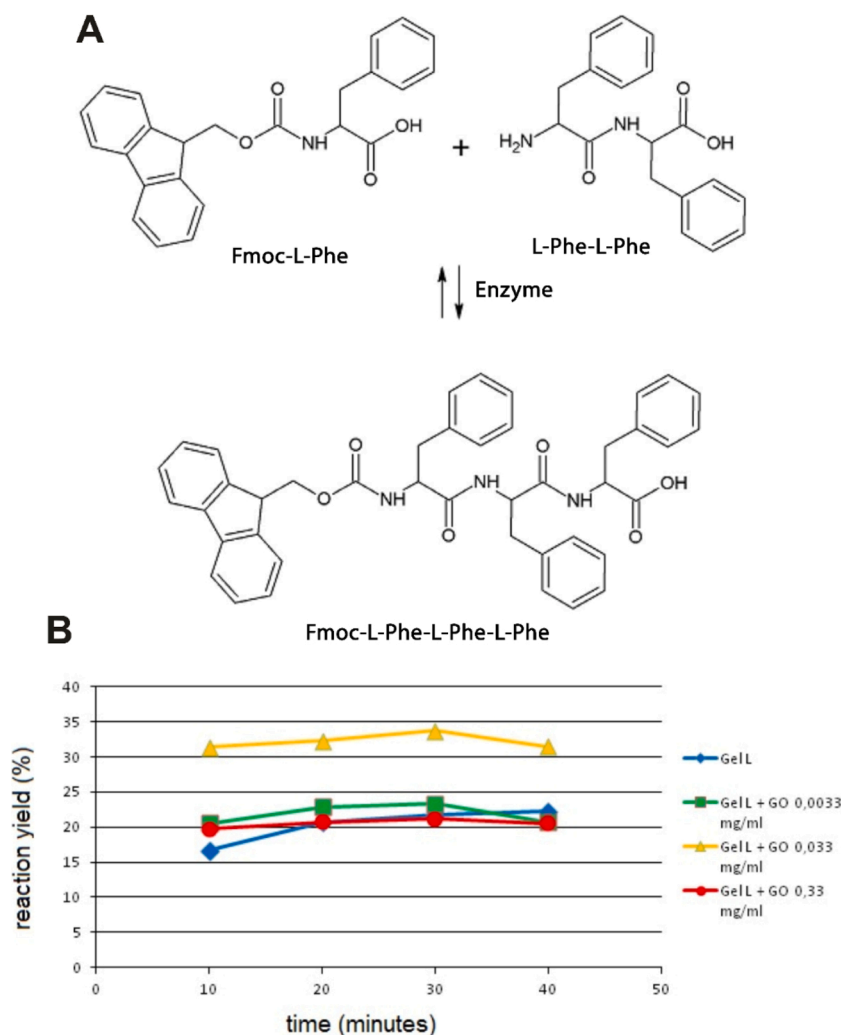
Fig. 1. (a) Reaction scheme of FmocPhe3 biosynthesis and (b) kinetics of FmocPhe3-GO composite hydrogel formation. Conversions are based on the HPLC peak areas at $\lambda = 256$ nm.

observed using a Zeiss Libra 120 transmission electron microscope (TEM).

For scanning electron microscopy (SEM), samples were deposited on aluminum stabs, air-dried and analyzed with a Zeiss Auriga 405 microscope at low extracting voltage (1.5–4 kV) and current (7.5 m aperture).

2.9. LIVE/DEAD cell viability assay

Synovial fluid Mesenchymal Stem Cells (Sf-MSCs) were isolated from synovial fluid collected from tibio-tarsal joints of 3 horses and cultured as described previously [27].

In a 96-well tissue culture dish, previously pre-treated with hydrogel composites with different GO concentration (0.033–0.333 mg/mL), Sf-MSCs were plated at a density of 10×10^3 cells/well in Dulbecco's Modified Eagle Medium (DMEM) supplemented with 10 % FCS. After 24 h, 48 h and 72 h of culture, cell viability was assayed by a LIVE/DEAD Viability/Cytotoxicity Assay kit (Life Technologies, Carlsbad, CA, USA). Samples were washed in PBS and then stained with a solution of 0.1μM calcein and 0.1 μM ethidium homodimer-1. Then, samples were washed with PBS and the fluorescent signal was measured using a fluorescent microplate Reader (GloMax Discover System, GM3000, Promega Corporation, Madison, WI, USA) at an excitation wavelength of 490 nm and an emission wavelength of 514 nm for the green color and an excitation wavelength of 528 nm and an emission wavelength 617 for the red color.

One-way analysis of variance (ANOVA) followed by Tukey's multiple comparison test were used to determine the p-value by the software GRAPH PAD PRISM 5.0 software (San Diego, CA, USA). The differences were considered significant at $p < 0.05$.

3. Results and discussion

3.1. Biosynthesis of hydrogel composites

A self-assembling hydrogel composite containing Fmoc-tripeptides and GO was synthesized through a reverse hydrolysis reaction, catalyzed by *P. fluorescens* lipase (Fig. 1a). In previous works, we have described and optimized the biosynthesis of FmocPhe3 hydrogels starting from FmocPhe and Phe2 precursors [25,28]. We have also demonstrated by LC–MS studies that in the presence of enzyme Fmoc-Phe3 is the most prominent reaction product and that no reaction takes place without enzyme [29]. Here, we have used such reaction to prepare hydrogel composites with different GO amounts.

In order to preliminarily evaluate the influence of the presence of GO on the enzymatic reaction, a series of hydrogel composites containing different amounts of GO were prepared and analyzed with HPLC, and the corresponding reaction yields were calculated. All the hydrogel composites resulted being self-supporting and GO did not interfere with the enzymatic reaction (data not shown). We subsequently studied the influence of GO on the kinetics of FmocPhe3 biosynthesis, for reaction
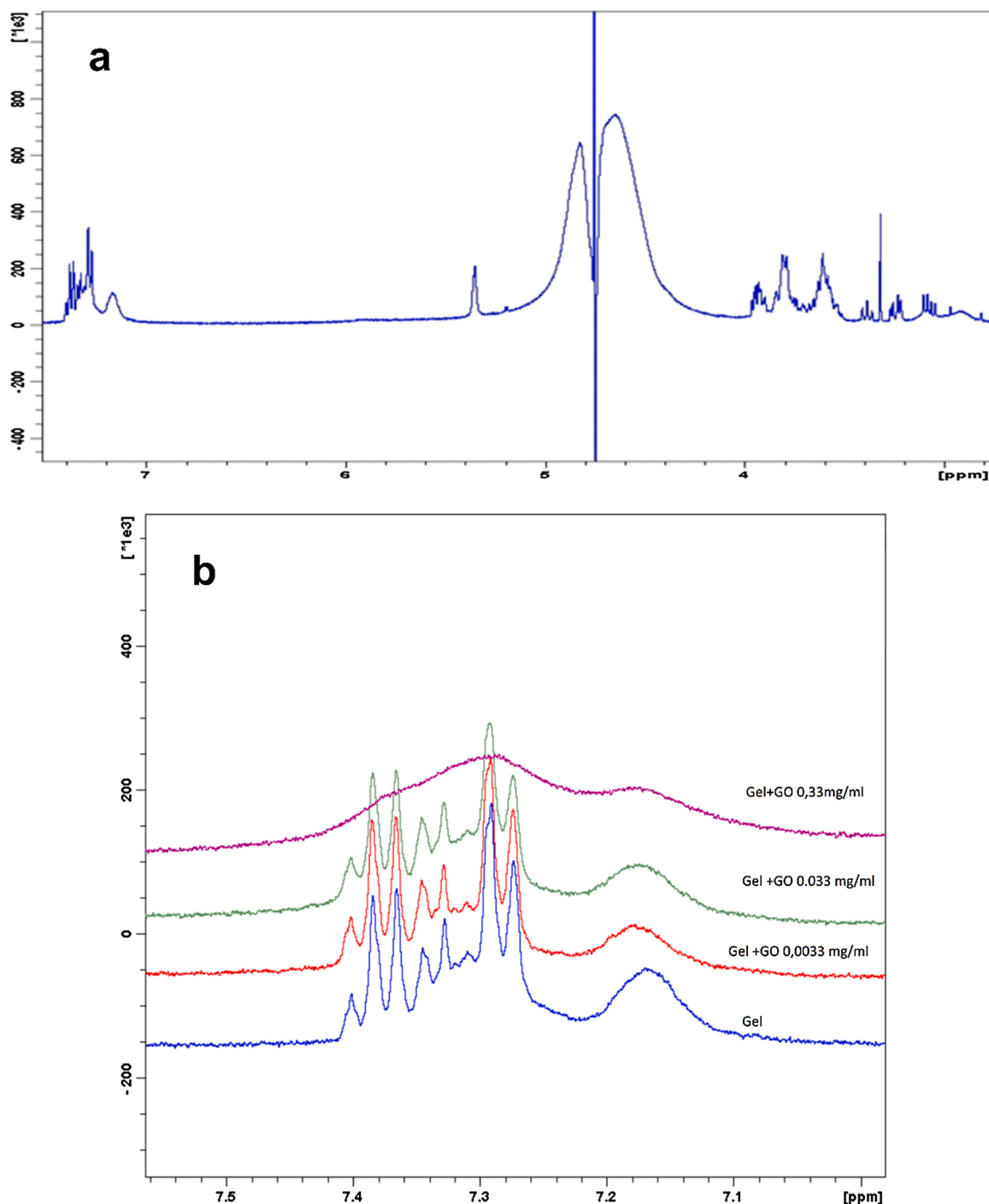
Fig. 2. (a) ^{1}HNMR spectrum of FmocPhe3 hydrogel and (b) aromatic part of the ^{1}HNMR spectra of hydrogel composites with different GO quantities.

times between 10 and 40 min. As shown in Fig. 1b, a plateau was reached within 20−30 min for all samples. For the composite with 0.033 mg/mL GO, the reaction yield reached ~33 %, while composites with different GO concentrations, as well as FmocPhe3 hydrogel, afforded reaction yields between 20 and 25 %. The presence of GO flakes during peptide gelation could favor the evolution of the reaction since the planar structure of GO molecules may interact with the peptide fibers via π-stacking. This effect may not be necessarily concentration dependent but under the experimental conditions used it seems to be optimal at [GO] =0.033 mg/mL. NMR was used to further investigate the interactions inside the composites. Fig. 2a reports the ^{1}HNMR spectrum of the native FmocPhe3 hydrogel. The peaks in the aromatic range of the

spectrum (7–7.6 ppm) correspond to the Fmoc group and Phe, while those in the aliphatic range (3–4 ppm) belong to Cα. The peaks appear wider and less defined than the corresponding peaks in the spectra of FmocPhe and Phe$_2$, due to a higher rigidity and stability of the molecules with a lower mobility due to hydrogel formation. Fig. 2b shows the aromatic parts of the spectra of hydrogel composites. By raising GO concentration, the peaks grow wider and less defined, which hints at a contribution of GO to the interactions among hydrogelators in the self-assembling process, in accordance with literature data that describe how low GO concentrations can remarkably affect the architecture of a hydrogel network [30].
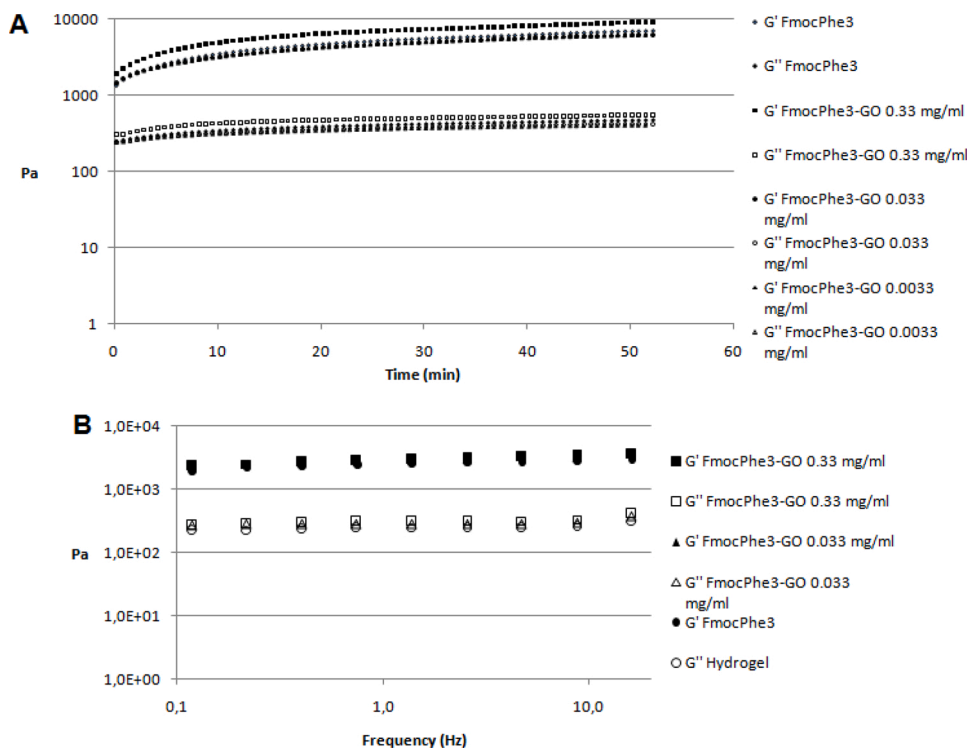
Fig. 3. A: Time evolution of Elastic (G') and viscous moduli (G'') for native and composite hydrogels with GO concentrations of 0.0033 mg/mL, 0.033 mg/mL and 0.33 mg/mL. B: Dependence of elastic (G') and viscous moduli (G'') on the applied frequency for native and composite hydrogels with GO concentrations of 0.033 mg/mL and 0.33 mg/mL.
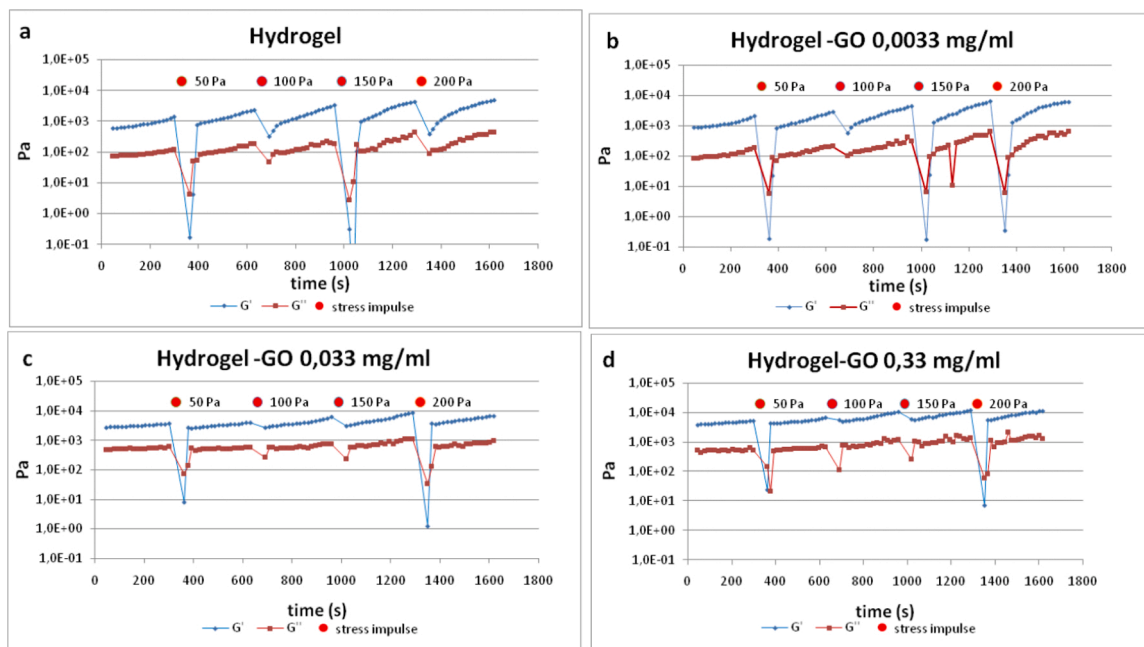

Fig. 4. Time evolution of G' (blue) and G'' (red) of native (a) and composite FmocPhe3 hydrogels with different GO concentrations (b: 0.0033 mg/mL, c: 0.033 mg/mL, d: 0.33 mg/mL) while applying an increasing stress impulse (50–200 Pa) every 5 min for 30 s.

3.2. rheological studies

The investigation of rheological properties of hydrogels is fundamental for evaluating their application potential in biotechnologies. The viscoelastic behavior of composite hydrogels with different GO contents after equilibrium was studied by rheological measurements and compared with the native FmocPhe₃ hydrogel. Fig. 3A reports the

evolution of G' and G'' over time, showing that both increased linearly as a function of reaction time, reaching a plateau after about 1 h. For all samples, already at the beginning of the reaction G' was significantly higher than G'', which is representative of a gel state. The crossover point between G' and G'' is not visible, indicating the occurrence of a fast reaction. After about 1 h the difference between G' and G'' was of about one order of magnitude for all samples. The composite hydrogel
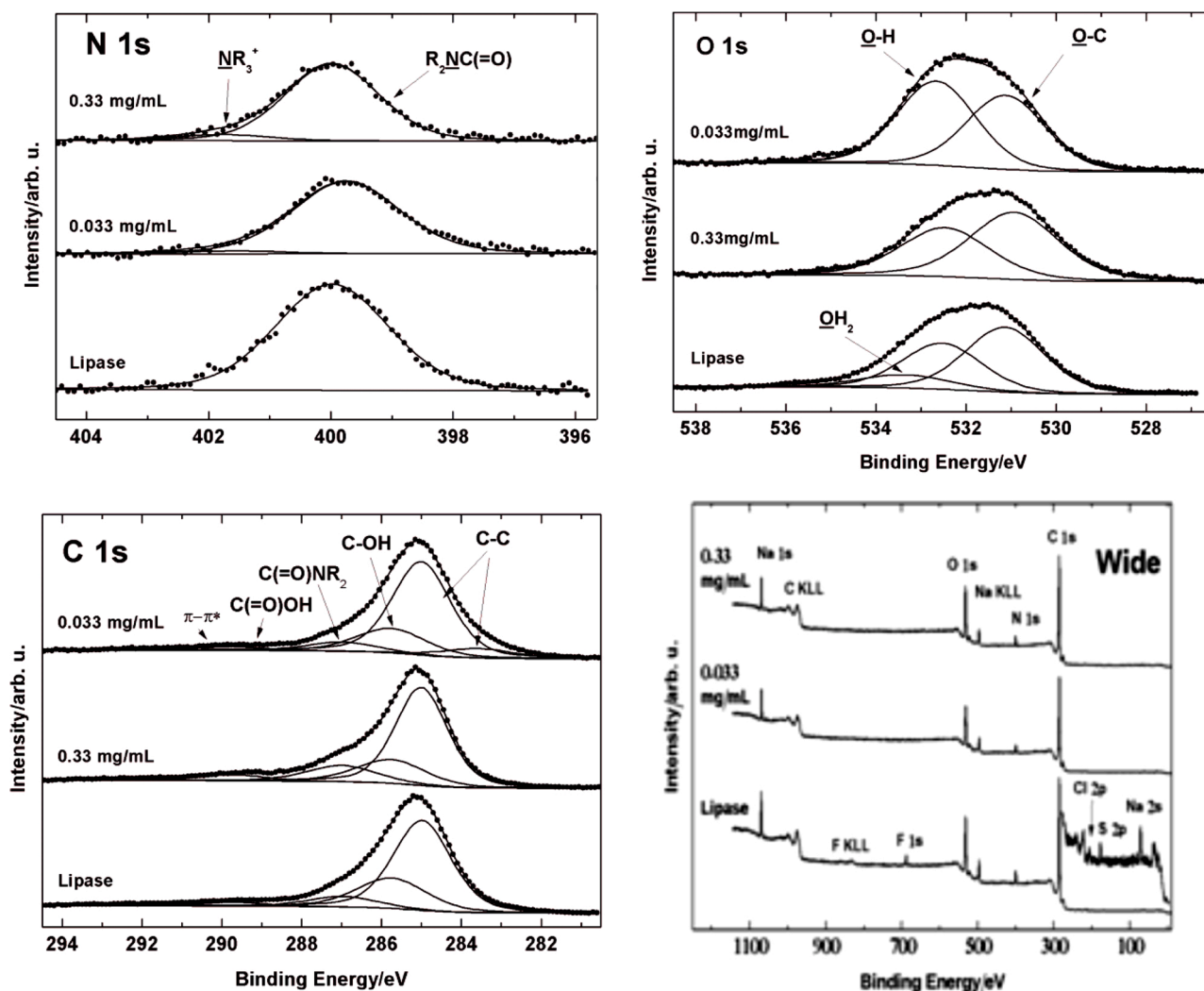
Fig. 5. Clockwise from bottom left: C1s, N1s, O1s and wide range XPS spectra of the hydrogels containing PFL before and after addition of 0.033 mg/mL or 0.33 mg/mL GO. All samples were mounted on stainless steel tips covered with freshly cleaved graphite foil.

with the highest GO concentration exhibited a greater values of G' and G'', while the native hydrogel and the other composites showed similar values. These results indicate the existence of synergetic interactions and good compatibility between GO and the hydrogel matrix, as reported in literature [31–33].

We attempted to evaluate the behavior of the composites when subjected to a growing stress impulse and their ability to recover (Fig. 4). The native hydrogel was stable for a limited period, before reaching a point where G' and G'' collapsed, indicating the hydrogel was broken. The material was able to restore its structure and viscoelastic properties in a short time. At higher GO concentrations (Fig. 4c and d), the hydrogels are more stable, with G' not dropping dramatically when increasing the shear stress. These results not only are fundamental for exploiting the hydrogels as injectable materials, but also demonstrate the strong interaction of GO flakes with the hydrogel structure, that stabilizes the composite.

3.3. XPS Measurements

XPS was used to characterize the hydrogels before and after addition of two different GO amounts. The commercial GO here employed was previously characterized in detail [34,35]. Summarizing, C1s in bare GO shows a convolution of peaks due to the contemporary presence of several functionalities: graphene sp^2 C atoms, C—C sp^3 bonds, hydroxyl,

epoxy, carbonyl and carboxyl groups, plus the high-lying satellite due to π-π* transition of aromatics. In the present case, where GO was added in moderate quantities to the hydrogel, the above features combine with those of the hydrogel. A rather simple wide-scan spectrum was obtained from the sample constituted by the hydrogel containing PFL, where the expected lines of C, O, N and Na plus weak contributions from S and Cl are present (F peaks are from the Teflon-covered tip) (Fig. 6). Despite the complexity of the enzyme, a single and symmetric N1s peak results, with a binding energy (BE) of 400.0 eV. A higher-lying component, possibly related to a cationic state of N and expected for zwitterions, results indistinguishable from the baseline. The proposed assignment of N1s is to amide groups, both from the absolute binding energies of N1s and O1s, and more reliably from the energy separation between the low-BE component of the complex O1s peak and the largely prevailing N1s peak component. In fact, the O1s signal contains, at increasing BEs, contributions from O—C bonds, hydroxyl groups and chemisorbed water. By taking into account the first one, the ON— difference amounts to 131.1–131.2 eV, a value which falls within the restricted range typical of amide groups [36]. The atomic ratio between O1s and N1s is 1.9, which evidences that such oxygen component is also due to other C—O functional groups. The C1s peak is complex, with a maximum at 285.0 eV. The other components can be assigned to hydroxyls (285.8), amides (287.0), carboxyl groups (289.7) and π-π* satellite peak (292.1) coming from FmocPhe. XPS results from hydrogels containing 0.033 mg/mL or
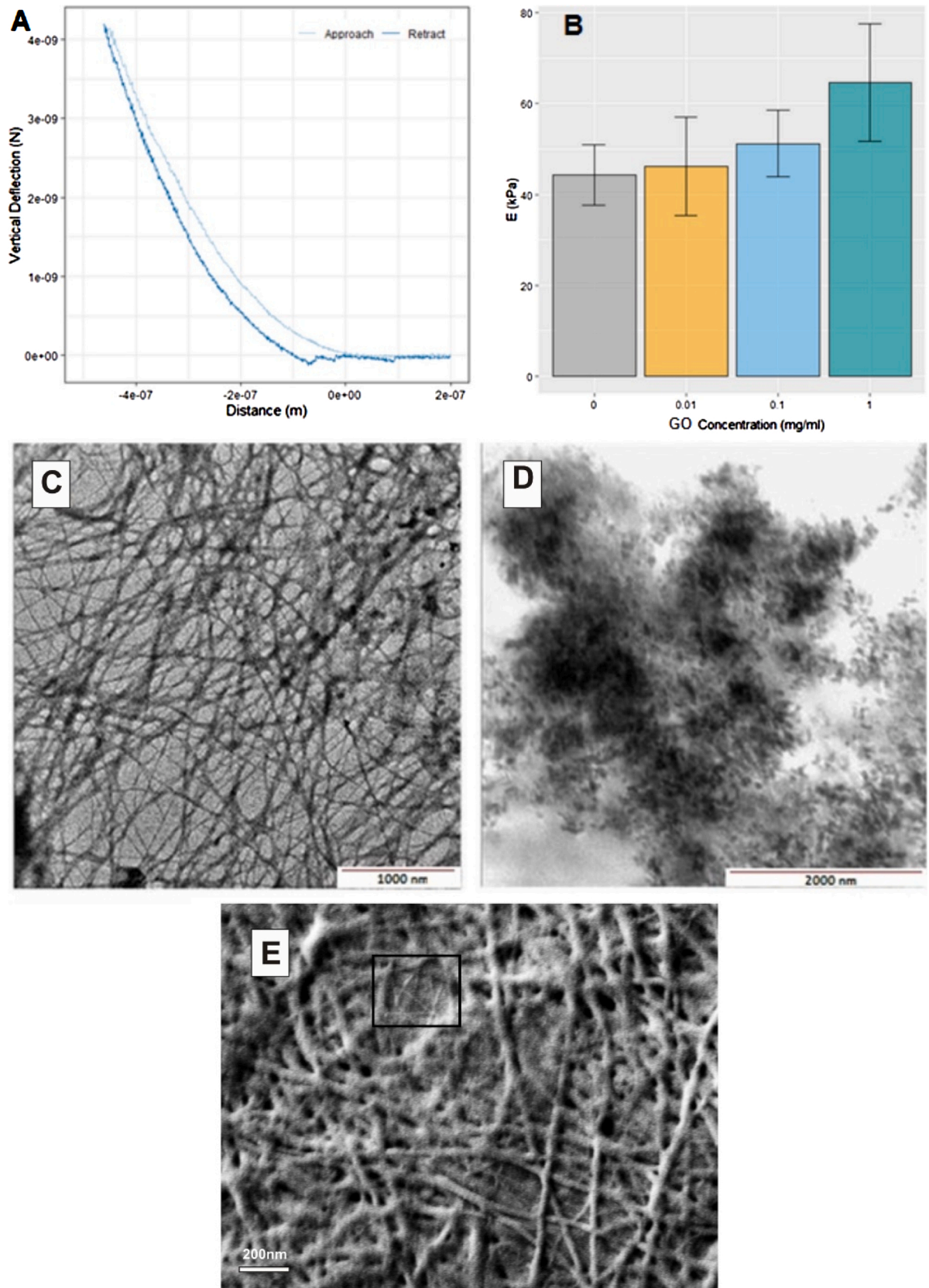
Fig. 6. A: typical AFM, FD cycles acquired on a native FmocPhe3 hydrogel; B: Average Young's modulus E with 95 % CI as a function of GO content; TEM image acquired on a native FmocPhe₃ hydrogel (C) and with a GO content of 0.33 mg/mL (D); E: SEM micrograph of a hydrogel-GO composite with GO concentration of 0.33 mg/mL. The black square indicates a GO lamella.
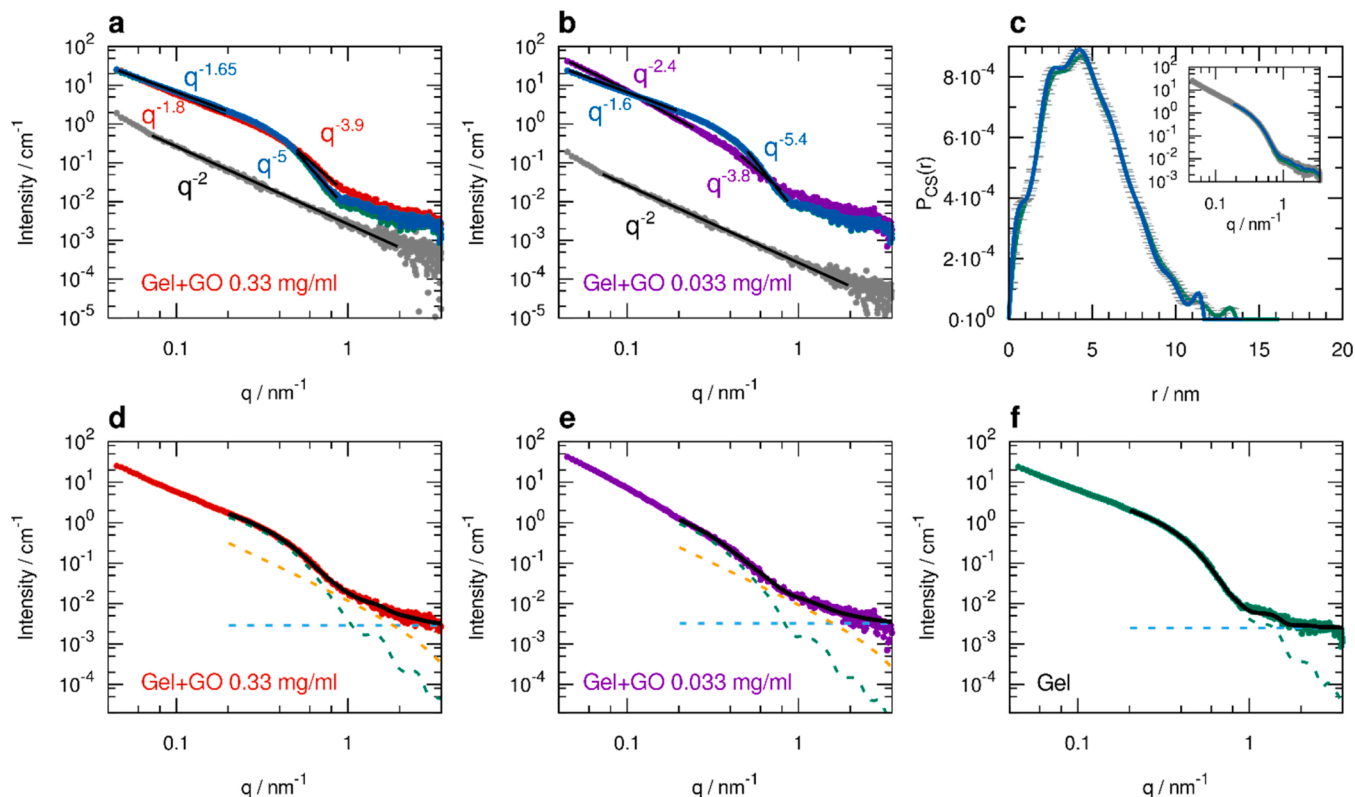
Fig. 7. a) experimental SAXS profiles of the native hydrogel (green dots), of the 0.33 mg/mL GO suspension (grey dots) and of the composite hydrogel containing 0.33 mg/mL GO (red dots) are compared to the simulated profile given by the simple sum of GO and hydrogel contributions (blue dots); b) same as in a) but considering the composite gel with GO 0.033 mg/mL (purple dots); c) Pair distance distribution functions of the cross section of the elongated fibrils which constitute the gel (green line). In the inset the fit to SAXS data provided by the indirect Fourier inversion is shown. The same analysis was performed on the data simulated considering the sum of the hydrogel and 0.33 mg/mL GO (blue line). d) model fit (black line) of the experimental data of the composite hydrogel with 0.33 mg/mL GO (red dots) considering a sum of a cylinder with elliptical cross-section (green dashed line) and a lamella contribution with 1 nm thickness (orange dashed line). The model parameters are reported in Table S1. The two separated form factors are shown as dashed lines, in addition to a flat background contribution (cyan dashed line); e) as in d) for the experimental data of the composite gel with 0.033 mg/mL GO (purple dots); f) model fit (black line) of the experimental data of the native hydrogel (green dots) considering a cylinder with elliptical cross-section (green dashed line) and a background contribution (cyan dashed line).

0.33 mg/mL GO are reported in Fig. 5. Wide scan spectra contain the same principal peaks reported for the native hydrogel. The N1s peak at 400.0 eV was the prevailing component for both samples, confirming the presence of amide groups as the largely prevailing components. A very weak component appears at higher BEs, which can be assigned to N^+states. The relative atomic ratios for C/N is 15.8 for both samples. This result calls for a homogenous surface composition of the resulting hydrogels.

3.4. Nano-mechanical measurements

The mechanical characterization of composite hydrogels with different GO content was studied by Indentation-Type Atomic-Force-Microscopy through the acquisition of FD cycles, composed of the approach and retract curves. In Fig. 6A, a typical FD cycle measured on a native hydrogel is reported. Fitting the Sneddon model to data, the local stiffness can be measured in terms of the Young's modulus E. To account for spatial inhomogeneity, eight 64-pixels E maps were acquired for each sample. Fig. 6B shows the average E for each sample. As expected, a hydrogel stiffening is observed increasing GO content. Consistently with rheological measurements, a similar mechanical response is observed for 0, 0.0033 and 0.033 mg/mL GO concentrations, with a more significant increase for the highest GO concentration. Large 95 % confidence intervals suggest a significant spatial heterogeneity of the mechanical properties within the same sample and among different samples.

3.5. TEM and SEM measurements

The morphological characterization of native and composite hydrogels with 0.33 mg/mL GO was conducted by TEM and SEM measurements. Fig. 6C reports TEM migrographs of native FmocPhe$_3$ gel with the presence of a nano-fibrillar network. These fibrils are several micrometers in length and their width is 40–60 nm. Unfortunately the corresponding TEM images of GO composite (Fig. 6D) do not clearly show the presence of GO sheets within the fibrillar hydrogel network. On the other hand SEM micrograph reported in Fig. 6E shows the presence of a composite hydrogel in which the fibrillar morphology is clearly displayed; it is also possible to see the presence of GO lamellae covered by fibers, giving evidence of GO incorporation within the peptide fibrillar network.

3.6. SAXS experiments

Small-angle X-ray scattering (SAXS) was used to assess changes in the structural morphology within composites compared to native hydrogels.

The experimental SAXS data of the GO suspension (Fig. 7a,b) confirmed the q^{-2} dependence of the scattered intensity expected for flat objects. No stacking peaks were observed suggesting that GO was fully dispersed in single sheets. The scattering profiles of the hydrogels showed the typical features of a fibrillar network [37]. At low-q a deviation from the ideal q^{-1} behavior expected for rigid rod-like structures was observed. In this q range longer range correlations determine more negative slopes of the scattering profile. As the samples were self-

standing gels, branching in the fibrillar network seemed to be the most reasonable explanation for this low-q upward scattering behavior. However, other reasons like fiber flexibility or the formation of large aggregates can give rise to similar effects on the scattering curve [37, 38]. Some changes in characteristic slopes were evident when comparing data between native and composite gels (Fig. 7a,b). Simulated profiles obtained by summing up the experimental data of GO in water and of the native gel failed to reproduce the experimentally observed profiles of the composites, suggesting that the observed changes could not be ascribed to a simple addition of the GO contribution. Therefore, the addition of GO implied a redistribution of the peptides in the composite.

In particular, we could observe that the characteristic low-q exponent increased in the composites compared to the native hydrogel, possibly due to an enhanced branching. The effect was more relevant for the composite with the lowest GO content (0.033 mg/mL). This non-monotonic trend with GO content suggests that above a certain fraction of GO, the interaction of large amounts of peptides with GO sheets can begin to be detrimental to network formation. The optimal GO content for preserving and enhancing the fibrillar network should be below the highest analyzed value (0.33 mg/mL) and reasonably not far from the lowest one (0.033 mg/mL).

A comparison of the curves in the larger q range related to the local structure ($0.5 < q < 1.5$ nm^{-1}) allowed us to appreciate that the composite gels showed a less negative slope, suggesting the presence, on average, of electron density contrast regions with smaller cross-section, since less steep decays of intensity as a function of q are associated with smaller characteristic distances. We focused on SAXS data at $q > 0.2$ nm^{-1} to remove the effect of branching and extract information on the local structure of the scattering particles. A preliminary analysis of the native hydrogel curve, based on indirect Fourier inversion method, allowed the extraction of a bell-shaped pair distance distribution of the fibril cross section with a peak around 4 nm (Fig. 7c). A model-based fitting procedure showed that the scattering curve was successfully reproduced by using the form factor of a long cylinder with an elliptical cross section with average minor and major axes of 7.4 and 13 nm, respectively (Table S1). When the composite gels with 0.033 mg/mL and 0.33 mg/mL GO concentrations were considered, we observed that a form factor comprising both the contribution of a long cylinder and a lamellar structure was needed to correctly describe the experimental data. The contribution of the lamellar structure is much larger than the one provided by GO in water alone and consistent with a lamellar thickness ≤ 1 nm. Also, for the composite gel with lower GO content, the fitting in the $q < 1$ nm^{-1} region required a slightly wider fibril cross section. In summary, SAXS results suggest that the composite gels maintain the structure of the native gel to a large extent. However, the fibril-forming material distributes partially with planar geometry, possibly due to direct interaction with GO lamellae. Moreover, the increased network branching and the estimated size of the fibrils cross section in the composite gel suggest that the native fibrils may partially associate in wider flat bundles, possibly induced by the interaction with GO, favoring the formation of "junction zones" of the fibrillar network with platelet-like geometry [37]. We can deduce that with a proper dose of GO doping the fibrillar network formed by the peptides is not totally destroyed and GO planes are well integrated in the composite by formation of layers of peptide material and junctions of native fibrils on them. This can possibly induce anisotropic mechanical properties[35] in the isotropic peptide hydrogel, which could be relevant in view of the application of these systems as injectable materials.

3.7. LIVE/DEAD assay

Previously published results have demonstrated the high compatibility of FmocPhe$_3$ hydrogels in the absence of GO [24,28].

In this work we investigated the induction of toxic effects in Sf-MSCs seeded on different hydrogel composites. After 24 h of cell culture, all
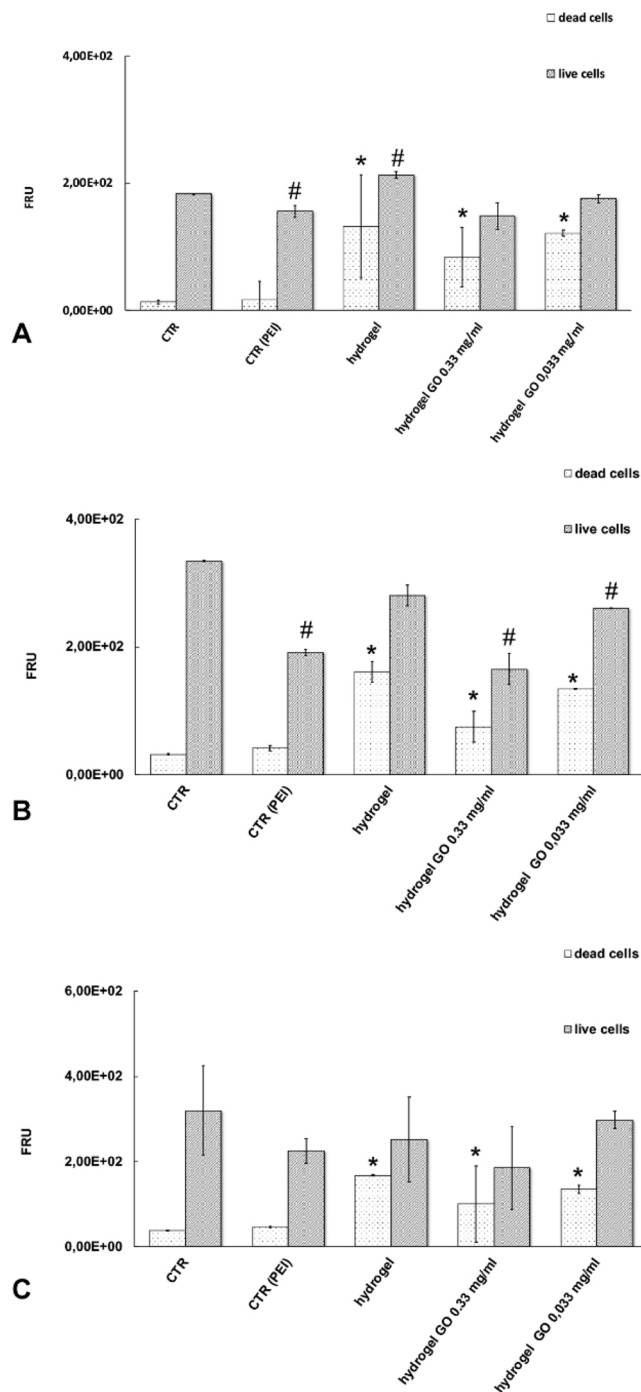

Fig. 8. Live/dead assay on sf-MSCs cultured on GO-hydrogel composites. (a) 24 h of cell culture; (b) 48 h of cell culture; (c) 96 h of cell culture. In all the experiments, control cells consisted in untreated cells (CTR) and cells exposed to the adhesive component (PEI). Data are expressed as mean Fluorescence Relative Units (FRU)$\pm$ SD (n = 3). * and # represent statistically significant differences with CTR samples (p < 0.05).

the different hydrogels tested did not significantly affect the viability of cells, although the level of dead cells increased compared to control samples (Fig. 8).

After 48 h (Fig. 1b) and 96 h (Fig. 1c) of cell growth, the evaluation of cell viability and cytotoxicity did not show any significant modifications, suggesting the lack of toxic events induced by different hydrogels and the compatibility of all the scaffolds with a long term exposition.

Moreover, we verified that the hydrogel composites do not induce

inflammatory responses in human blood cells (Fig. S1), that appears of interest for future applications within vascularized tissues.

4. Conclusions

In this work, we developed an innovative hydrogel composite formulation, based on FmocPhe$_3$ and GO nanosheets [39]. Hydrogel biosynthesis was not hindered by the presence of GO and the composite hydrogels [40] largely maintained the fibrillar network structure of the native FmocPhe3 hydrogel. The optimization of the GO amount (at 0.033 mg/mL) resulted in a good integration of GO planes in the composite, that afforded a material with improved mechanical properties that appears suitable for the future development of advanced biotechnological applications [41].

Funding

Author contributions

Laura Chronopoulou: Methodology, Visualization, Writing - original draft, Writing - review & editing.
Antonio Di Nitto: Investigation, Visualization.
Massimiliano Papi: Resources, Writing - original draft.
Ornella Parolini: Funding acquisition, Project administration.
Mirella Falconi: Resources.
Gabriella Teti: Investigation.
Aurelio Muttini: Resources.
Wanda Lattanzi: Resources, Writing - original draft.
Valentina Palmieri: Investigation.
Gabriele Ciasca: Investigation.
Alessandra Del Giudice: Investigation, Visualization, Writing - original draft.
Luciano Galantini: Resources, Methodology.
Robertino Zanoni: Resources, Funding acquisition, Investigation.
Cleofe Palocci: Conceptualization, Supervision, Writing - review & editing.

Declaration of Competing Interest

The authors declare that they have no known competing financial interests or personal relationships that could have appeared to influence the work reported in this paper.

Acknowledgements

Appendix A. Supplementary data

Supplementary material related to this article can be found, in the online version, at doi:https://doi.org/10.1016/j.colsurfb.2021.111989.

References

[1] M.W. Tibbitt, J.E. Dahlman, R. Langer, Emerging frontiers in drug delivery, J. Am. Chem. Soc. 138 (2016) 704–717.

[2] M.W. Tibbitt, C.B. Rodell, J.A. Burdick, K.S. Anseth, Progress in material design for biomedical applications, PNAS 112 (2015) 14444–14451.

[3] J.D. Kretlow, S. Young, L. Klouda, M. Wong, A.G. Mikos, Injectable biomaterials for regenerating complex craniofacial tissues, Adv. Mater. 21 (2009) 3368–3393.

[4] J.B. Wolinsky, Y.L. Colson, M.W. Grinstaff, Local drug delivery strategies for Cancer treatment: gels, nanoparticles, polymeric films, rods, and wafers, J. Control. Release 159 (2012) 14–26.

[5] J.S. Temenoff, A.G. Mikos, Injectable Biodegradable Materials for Orthopedic Tissue Engineering, Biomaterials 21 (2000) 2405–2412.

[6] J.D. Kretlow, L. Klouda, A.G. Mikos, Injectable matrices and scaffolds for drug delivery in tissue engineering, Adv. Drug Deliv. Rev. 59 (2007) 263–273.

[7] J.K. Sahoo, M.A. VandenBerg, M.J. Webber, Injectable network biomaterials via molecular or colloidal self-assembly, Adv. Drug Deliv. Rev. 127 (2018) 185–207.

[8] G.M. Whitesides, B. Grzybowski, Self-assembly at all scales, Science 295 (2418-) (2002) 2421.

[9] J. Wang, K. Liu, R. Xing, X. Yan, Peptide self-assembly: thermodynamics and kinetics, Chem. Soc. Rev. 45 (2016) 5589–5604.

[10] A. Oryan, A. Kamali, A. Moshiri, H. Baharvand, H. Daemi, Chemical crosslinking of biopolymeric scaffolds: current knowledge and future directions of crosslinked engineered bone scaffolds, Int. J. Biol. Macromol. 107 (2018) 678–688.

[11] T.R. Hoare, D.S. Kohane, Hydrogels in drug delivery: progress and challenges, Polymer 49 (2008) 1993–2007.

[12] W.Y. Seow, C.A.E. Hauser, Short to ultrashort peptide hydrogels for biomedical uses, Mater. Today 17 (2014) 381–388.

[13] R. Yegappan, V. Selvaprithiviraj, S. Amirthalingam, R. Jayakumar, Carrageenan based hydrogels for drug delivery, tissue engineering and wound healing, Carbohydr. Polym. 198 (2018) 385–400.

[14] K. Varaprasad, G.M. Raghavendra, T. Jayaramudu, M.M. Yallupu, R. Sadiku, A mini review on hydrogels classification and recent developments in miscellaneous apllications, Mater. Sci. Eng. C 79 (2017) 958–971.

[15] M.W. Tibbitt, K.S. Anseth, Hydrogels as extracellular matrix mimics for 3D cell culture, Biotechnol. Bioeng. 104 (2009) 655–663.

[16] S. Toledano, R.J. Williams, V. Jayawarna, R.V. Ulijn, Enzyme-triggered self-assembly of peptide hydrogels via reversed hydrolysis, J. Am. Chem. Soc. 128 (4) (2006) 1070–1071.

[17] J.K. Wychowaniéc, M. Iliut, M. Zhou, J. Moffat, M.A. Elsawy, W.A. Pinheiro, J. A. Hoyland, A.F. Miller, A. Vijayaraghavan, A. Saiani, Designing Peptide/Graphene hybrid hydrogels through fine-tuning of molecular interactions, Biomacromolecules 19 (2731-) (2018) 2741.

[18] J.W. Suk, R.D. Piner, J. An, R.S. Ruoff, Mechanical properties of monolayer graphene oxide, ACS Nano 4 (2010) 6557–6564.

[19] A.G. Marrani, R. Zanoni, R. Schrebler, E.A. Dalchiele, Toward Graphene/Silicon Interface via Controlled Electrochemical Reduction of Graphene Oxide, J. Phys. Chem. C 121 (2017) 5675–5683.

[20] W. Gao, L.B. Alemany, L. Ci, P.M. Ajayan, New insights into the structure and reduction of graphite oxide, Nat. Chem. 1 (2009) 403–408.

[21] Y. Wu, B.O. Okesola, J. Xu, I. Korotkin, A. Berardo, I. Corridori, F.L. Pellerej di Brocchetti, J. Kanczler, J. Feng, W. Li, Y. Shi, V. Farafonov, Y. Wang, R. F. Thompson, M.M. Titirici, D. Nerukh, S. Karabasov, R.O.C. Oreffo, J. C. Rodriguez-Cabello, G. Vozzi, H.S. Azevedo, N.M. Pugno, W. Wang, A. Alvaro Mata, Nat. Commun. 11 (2020) 1182–1194.

[22] C. Ligorio, M. Zhou, J.K. Wychowaniec, X. Zhu, C. Bartlam, A.F. Miller, A. Vijayaraghavan, J.A. Hoyland, A. Saiani, Acta Biomater. 92 (2019) 92–103.

[23] P. Xing, C. Chiaoxiao, S. Li, M. Ma, A. Hao, Hybrid gels assembled from fmoc-amino acid and graphene oxide with controllable properties, Chem. Phys. Chem. 15 (2014) 2377–2385.

[24] L. Chronopoulou, A.R. Togna, G. Guarguaglini, G. Masci, F. Giammaruco, G. I. Togna, C. Palocci, Self-assembling peptide hydrogels promote microglial cells proliferation and NGF production, Soft Matter 8 (2012) 5784–5790.

[25] L. Chronopoulou, S. Sennato, F. Bordi, D. Giannella, A. Di Nitto, A. Barbetta, M. Dentini, A.R. Togna, G.I. Togna, S. Moschini, C. Palocci, Designing unconventional fmoc peptide-based biomaterials: structure and related properties, Soft Matter 10 (2014) 1944–1952.

[26] S. Hansen, BayesApp : a web site for indirect transformation of small-angle scattering data, J. Appl. Crystallogr. 45 (2012) 566–567.

[27] E. Mazzotti, G. Teti, M. Falconi, F. Chiarini, B. Barboni, A. Mazzotti, A. Muttini, Age-related alterations affecting the chondrogenic differentiation of synovial fluid mesenchymal stromal cells in an equine model, Cells 8 (2019) 1116.

[28] L. Chronopoulou, S. Lorenzoni, G. Masci, M. Dentini, A.R. Togna, G.I. Togna, F. Bordi, C. Palocci, Lipase-supported synthesis of peptidic hydrogels, Soft Matter 6 (2010) 2525–2532.

[29] L. Chronopoulou, M. Daniele, V. Perez, A. Gentili, T. Gasperi, S. Lupi, C. Palocci, A physico-chemical approach to the study of genipin crosslinking of biofabricated peptide hydrogels, Process. Biochem. 70 (2018) 110–116.

[30] Y. Huang, M. Zeng, Z. Feng, D. Yin, Q. Xua, L. Fana, Graphene oxide-based composite hydrogels with self-assembled macroporous structures, RSC Adv. 6 (2016) 3561–3570.

[31] Y. Huang, M. Zeng, J. Chen, Y. Wang, Q. Xu, Multi-structural network design and mechanical properties of graphene oxide filled chitosan-based hydrogel nanocomposites, Mater. Des. 148 (2018) 104–114.

[32] J. Nath, A. Chowdhury, S.K. Kumar Dolui, Chitosan/graphene oxide-based multifunctional pH-responsive hydrogel with significant mechanical strength, self-healing property, and shape memory effect, Adv. Polym. Technol 37 (2018) 3665–3679.

[33] Z. Wang, J. Li, L. Jiang, S. Xiao, Y. Liu, J. Luo, Zwitterionic hydrogel incorporated graphene oxide nanosheets with improved strength and lubricity, Langmuir 35 (2019) 11452–11462.

[34] A.G. Marrani, R. Zanoni, R. Schrebler, E.A. Dalchiele, J. Phys.Chem. C 121 (2017) 5675–5683.

[35] V. Palmieri, E.A. Dalchiele, G. Perini, A. Motta, M. De Spirito, R. Zanoni, A. G. Marrani, M. Papi, Chem. Commun. 55 (2019) 4186–4189.

[36] G. Beamson, D. Briggs, High Resolution XPS of Organic Polymers, the Scienta ESCA300 Database, Wiley, Chichester, 1992. ISBN 0471 935921.

[37] P. Térech, Molecular gels and small-angle scattering. Molecular Gels: Materials with Self-assembled Fibrillar Networks, Springer-Verlag, Berlin, 2006, pp. 275–324.

[38] Y. Kudo, et al., Flexibility and local structure of a worm-like cylinder of self-assembled discotic triazine triamide, Polym. J. 42 (2010) 812–817.

[39] S.C. Boothroyd, et al., Controlled structure evolution of graphene networks in polymer composites, Chem. Mater. 30 (2018) 1524–1531.

[40] X. Wu, Y. Xing, K. Zeng, K. Huber, J.X. Zhao, Study of fluorescence quenching ability of graphene oxide with a layer of rigid and Tunable silica spacer, Langmuir 34 (2018) 603–611.

[41] A. Paul, A. Hasan, H. Al Kindi, A.K. Gaharwar, V.T.S. Rao, M. Nikkhah, S.R. Shin, D. Krafft, M.R. Dokmeci, D. Shum-Tim, A. Khademhosseini, Injectable graphene Oxide/Hydrogel-Based angiogenic gene delivery system for vasculogenesis and cardiac repair, ACS Nano 8 (2014) 8050–8062.